Journal of Nanobiotechnology

RESEARCH

Open Access

Concurrent induction of pyroptosis and immunogenic cell death by capsaicin/graphene nanocomplex for enhanced breast cancer immunotherapy

Silu Li[1,2†], Xin Jin[1,2†], Yumo Zhang[2], Jidan Huang[2], Haiqiang Wang[2], Huan Meng[2*], Jiulong Li[2*] and Lin Zhu[1*]

Abstract

Inducing immunogenic cell death (ICD) has emerged as a promising strategy for targeting immunologically "cold" tumors. However, most current therapies focus on a single mechanism, limiting their efficacy. In this study, we propose a nano-enabled approach that synergistically activates two complementary immunogenic killing mechanisms: pyroptosis, which elicits a potent inflammatory response, and ICD, characterized by the presentation of 'eat-me' signals and tumor antigens to the immune system. Capsaicin, a naturally occurring compound, was employed to induce pyroptosis via ROS-mediated gasdermin E (GSDME) cleavage, resulting in cell membrane blebbing and subsequent cell death. To simultaneously trigger ICD, we incorporated 2D graphene oxide (GO) engineered with optimized physicochemical properties to induce robust ICD under near-infrared irradiation. Our in vitro and in vivo experiments demonstrated that the combined treatment of capsaicin and GO not only enhanced cancer cell killing but also promoted immune cell infiltration and potentiated anti-tumor immunity, leading to significant tumor suppression. Moreover, the dual-trigger mechanism of pyroptosis and ICD yielded superior anti-tumor efficacy compared to single-modality treatments while maintaining a favorable biosafety profile. These findings highlight the potential of a synergistic nano-enabled strategy for improving cancer immunotherapy.

Keywords Cancer immunotherapy, Pyroptosis, Immunogenic cell death, Combination therapy, Capsaicin

[†]Silu Li and Xin Jin have contributed equally to this work.

*Correspondence:
Huan Meng
mengh@nanoctr.cn
Jiulong Li
lijl@nanoctr.cn
Lin Zhu
zhulin66zhulin@163.com

Graphical Abstract

Concurrent Pyroptosis and ICD Induction via Cap/GO Synergy Enhances Anti-Tumor Immunity. The Cap/GO complex combines ROS-mediated pyroptosis (via Cap) with ICD activation (via GO under NIR irradiation), fostering an immunological tumor microenvironment. Pyroptosis triggers IL-6 and IL-1β, while ICD exposes CRT and HMGB1. This synergy drives T-cell infiltration, amplifying anti-tumor immunity and achieving robust tumor suppression.

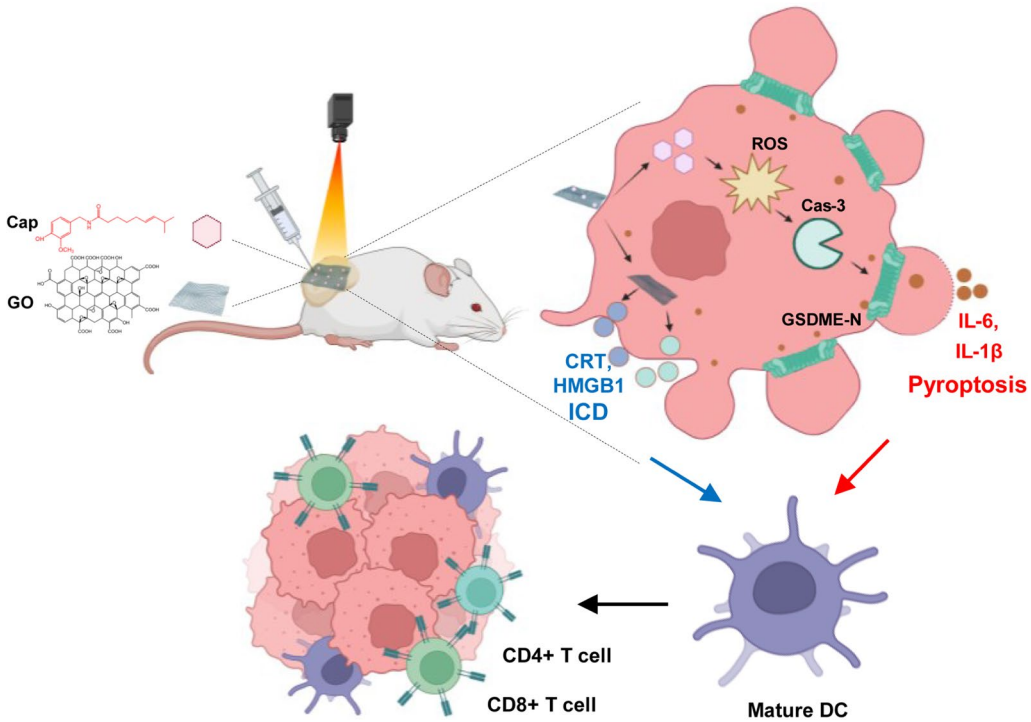

Introduction

Immunotherapy has revolutionized cancer treatment by leveraging the immune system's ability to recognize and kill malignant cells. However, its clinical success in breast cancer (BC) has been limited, especially in the context of "cold" BC tumors, which generally exhibit low immune cell infiltration and poor immunogenicity [1–4]. To address this challenge, there is increasing interest in developing novel strategies to enhance the immunogenicity of cancer cells and promote a pro-inflammatory tumor microenvironment. While most forms of cell death, such as apoptosis, are considered non-immunogenic and often fail to elicit an immune response, certain types, such as immunogenic cell death (ICD), ferroptosis, certain types of necroptosis, and more recently pyroptosis, are highly immunogenic [5–7]. ICD exposes tumor antigens and releases danger-associated molecular patterns (DAMPs), which act as 'eat-me' signals to the immune system [7]. Pyroptosis, on the other hand, is a highly inflammatory form of cell death, characterized by the release of pro-inflammatory cytokines (such as IL-1β, IL-18, and IL-6), which further amplify immune activation [6, 8]. While pyroptosis shares several characteristics with ICD, including the release of DAMPs such as HMGB1 and ATP, it may not sufficiently activate adaptive immunity on its own due to limited antigen presentation. In contrast, classical ICD promotes calreticulin (CRT, an endogenous antigen) exposure, as well as the release of HMGB1 and ATP serve as endogenous adjuvants. Ample evidence has demonstrated the benefits of using small molecules (e.g., use of paclitaxel to stimulate high mobility group protein B1 (HMGB1) in a 4T1 mouse model) [6, 8], peptides (e.g., use of PKHB1 peptide to induce ROS production in a 4T1 mouse model) [9, 10], radiation (e.g., use of X-rad to trigger immune activation in PyMT model) [11], or nanoparticles (e.g., use of mitoxantrone-laden liposome to trigger a robust immune response in EMT6 and 4T1 tumor model) to induce ICD [12], yielding promising immunological outcomes

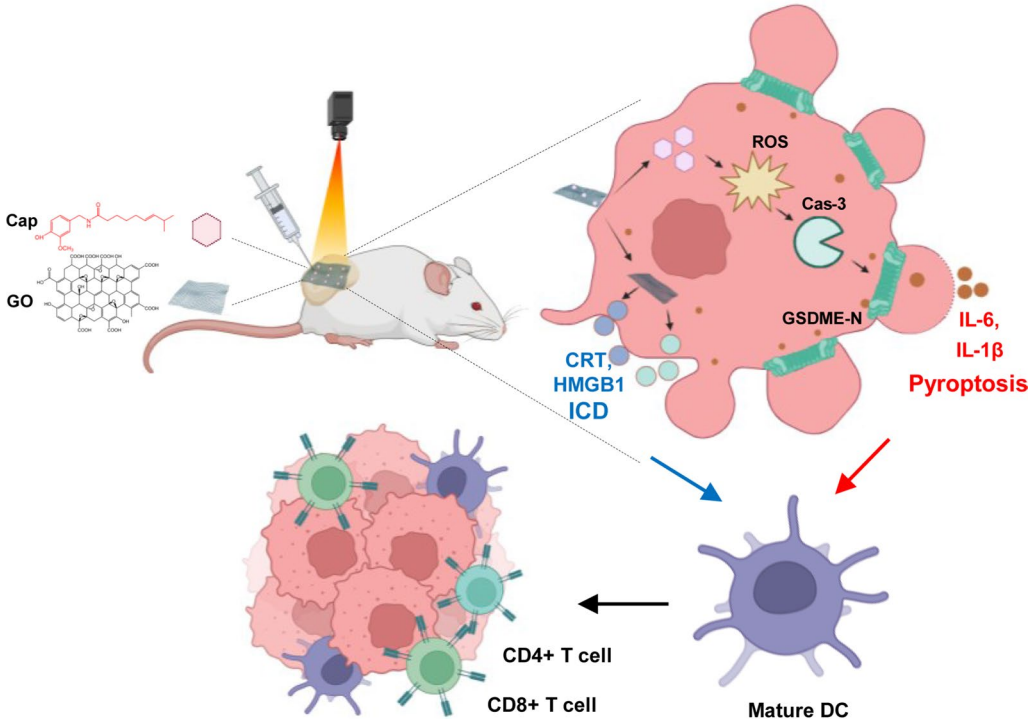

Scheme 1 Schematic diagram of the antitumor mechanism of Cap/GO nanocomplex. Capsaicin (Cap), a natural compound that induces ROS-mediated pyroptosis, is mixed with graphene oxide (GO) due to presented π–π stacking, which facilitates ICD under NIR irradiation. Intratumoral injection of this physically combined Cap/GO nanocomplex triggers both pyroptosis and ICD concurrently, generating an immunological tumor microenvironment enriched with IL-6 and IL-1β from pyroptosis, along with immune-activating signals CRT and HMGB1 from ICD. This combined immune response enhances the infiltration and activation of $CD4^+$ and $CD8^+$ T cells, leading to robust anti-tumor immunity and significant tumor suppression

in breast cancer models. Despite these advances, most strategies focus on a single immunogenic killing mechanism, leaving the potential for synergistic effects between multiple mechanisms underexplored in BC treatment. We hypothesize that combining distinct and complementary forms of immunogenic killing mechanisms could offer a powerful therapeutic advantage. By not only directly eliminating tumor cells but also converting cold tumors into "hot" tumors, this strategy could enhance immune cell infiltration and significantly amplify the overall anti-tumor immune response.

The combination of ICD and pyroptosis presents a compelling strategy for cancer immunotherapy due to their complementary mechanisms and synergistic effects in transforming cold tumors into "hot" tumors. ICD enhances pyroptosis by releasing DAMPs and tumor-specific antigens, facilitating the recognition of cancer cells by the immune system through 'eat-me' signals. According to an established consensus, key biomolecules associated with ICD include the expression of calreticulin (CRT) and the release of HMGB1 and ATP [13]. In parallel, pyroptosis induces the release of pro-inflammatory cytokines, creating a favorable immunological tumor microenvironment that attracts and activates immune cells, further enhancing anti-tumor immunity [14]. These dual mechanisms effectively disrupt the immunosuppressive tumor microenvironment, inducing robust local immune responses while supporting systemic anti-tumor immunity.

Against this background, we synthesized a nanocomplex capable of concurrently inducing pyroptosis and ICD. Due to its potent immunostimulatory effects, accessibility, and synergistic potential, we selected the natural product capsaicin (Cap), which is FDA-approved for topical use in over-the-counter creams or patches [15–17]. This is a naturally occurring compound, also known as (*E*)-*N*-(4-Hydroxy-3-methoxybenzyl)−8-methylnon-6-enamide, serendipitously discovered to induce pyroptosis following cellular screening across various cancer cell types. Additionally, we engineered graphene oxide (GO) variants with different sizes (~500, ~1000, and ~1500 nm) and surface modifications (C=O content of ~5%, ~10%, and ~15%) to identify the most effective formulation for inducing ICD upon 808 nm irradiation. Notably, the C=C-rich structures in both GO and Cap (that contain the benzyl group) enabled the synthesis of a Cap/

GO nanocomplex, designed to simultaneously induce pyroptosis and ICD. The resulting nanocomplex capitalizes on the dual mechanisms of cell death to directly eliminate tumor cells while enhancing anticancer immunity (Scheme 1), presenting a promising strategy for more effective and durable cancer treatments in an EMT-6 syngeneic model, a widely used model for studying breast cancer immunotherapy.

Results and discussion

Efficient induction of pyroptosis by capsaicin

Capsaicin (*E*)-*N*-(4-Hydroxy-3-methoxybenzyl, Cap), a homovanillic acid derivative in chili peppers, has emerged as a valuable source of compounds for drug development due to its analgesic, antioxidant, anti-inflammatory, or anticancer properties [15–17]. While our initial aim was to study its immunomodulatory effects in a dermal application, we made a serendipitous discovery: Cap triggered a robust pyroptosis response, as detailed below. We also included Cap analogs, arvanil (Arv) and olvanil (Olv), which differ in carbon chain length and degrees of unsaturation, in our study. We first evaluated the cytotoxicity on the mouse BC cell lines, EMT6 and Py8119, as well as the osteosarcoma cell line, K7M2. The results, as depicted in Fig. 1A, showed a clear concentration-dependent decrease in cell viability for all three compounds across all cell lines over a dose range of 0–200 μg/mL. Although Cap and its analogs displayed similar IC_{50} values, they induced significant morphological changes in these cell lines under 50 μg/mL (denoted as "l") or 100 μg/mL (denoted as "h"), including pronounced cell swelling and large surface blebbing (Fig. 1B), hallmarks of pyroptotic cell death. This was comparable to the effects observed with the positive control, doxorubicin (Dox). We further investigated Cap-induced pyroptosis using the Operetta High Content Screening System (Perkin Elmer) in conjunction with Annexin V-fluorescein isothiocyanate (FITC) and propidium iodide (PI) fluorescence staining, a method widely recognized for characterizing pyroptosis through extensive membrane damage and phosphatidylserine externalization [18]. A time-lapsed video (Movie 1) and sequential confocal images collected from 0 to 1000 min (Fig. 1C) captured the dynamics of Cap-induced morphological changes, revealing a time-dependent increase in both PI and Annexin V staining. We observed a pronounced increase in PI-positive and Annexin V-positive cell populations at 760 min (Fig. 1C). Additionally, we repeated the PI and Annexin V staining in Py8119 and K7M2 cells, which demonstrated an even faster induction of pyroptosis, occurring at 540 min (Fig. 1D).

At the molecular level, we investigated the expression of the pyroptosis marker Gasdermin E cleavage (GSDME-NT) after incubating EMT6 cells with Cap and its analogs. Since GSDME cleavage is an upstream event relative to compromised cell membrane integrity (indicated by PI positivity at 720 min), we deliberately chose a 420-min (7-h) incubation period for EMT6 cells. Western blot (WB) results (Fig. 1E) demonstrated a significant increase in GSDME-NT expression at various concentrations (50 μg/mL and 100 μg/mL, denoted as "l" and "h") without significant effect on GSDMD cleavage (Figure S1), indicating strong activation of cell death through a GSDME-mediated pyroptotic pathway. The phenomenon in which GSDME-NT levels are highest at lower drug concentrations and decline at higher doses could be attributed to the fact that, as drug concentrations increase, extensive cell death occurs through multiple pathways. This leads to rapid cell lysis and protein degradation, preventing the accumulation of GSDME-NT. Mechanistically, given Cap's established effects on mitochondria-based reactive oxygen species (ROS) production and plasma membrane NADH oxidase activity [17], we assessed intracellular ROS levels using the H_2DCFDA assay, which evaluates both plasma membrane and mitochondrial ROS [18, 19]. H_2O_2 served as a positive control.

(See figure on next page.)

Fig. 1 Induction of cancer cell pyroptosis by natural product Cap in vitro and in vivo. **A** Chemical structures of Cap, Arv, and Olv, and their cell-killing effects on the breast cancer cell lines EMT6 and Py8119 and the osteosarcoma cell line K7M2 after 24 h incubation. **B** Representative optical microscope images to compare the EMT6 cell morphological changes induced by various concentrations of Cap, Arv, and Olv. "l" represents a low concentration of 50 μg/mL, and "h" represents a high concentration of 100 μg/mL. Dox is used as a positive control. Red arrows indicate the swollen and blebbing cells. The scale bar is 25 μm. **C** Representative confocal images acquired on an Operetta High Content Screening System (Perkin Elmer) to demonstrate the dynamics of capsaicin-induced morphological and fluorescence intensity changes of EMT6 cells from 0 to 1000 min incubation time. Annexin V-FITC and PI were added to the cells before imaging. **D** Fluorescent images to demonstrate the Cap-induced morphological and fluorescence intensity changes in Py8119 and K7M2 cells. **E** Western blotting to show the cleavage of GSDME-FL to GSDME-NT in EMT6 cells treated by 50 (l) and 100 (h) μg/mL of Cap and its analogs Arv and Olv for 7 h. Quantitative analysis of GSDME-NT expression intensities was calculated by ImageJ software. **F** H_2DCFDA assay to evaluate the intracellular ROS by Cap, Arv, and Olv in EMT6 cells. **G** ELISA assays to determine the released LDH (top panel) and IL-6 (upper panel) levels in cells. **H** Immunoblotting to demonstrate the GSDME-NT cleavage and cleaved caspase-3 expression levels in EMT6-bearing mice after 3 days of 5 mg/kg Cap intratumoral injection. The ratios of GSDME-NT/Vinculin and cleaved caspase-3/Vinculin in different treatment groups were calculated by Image J. **I** Determination of IL-6 (top panel) and IL-1β (upper panel) in EMT6-bearing mouse serum using ELISA assays. Data represents mean ± SD, $n \geq 3$. * $p < 0.05$, ** $p < 0.01$, *** $p < 0.001$, **** $p < 0.0001$

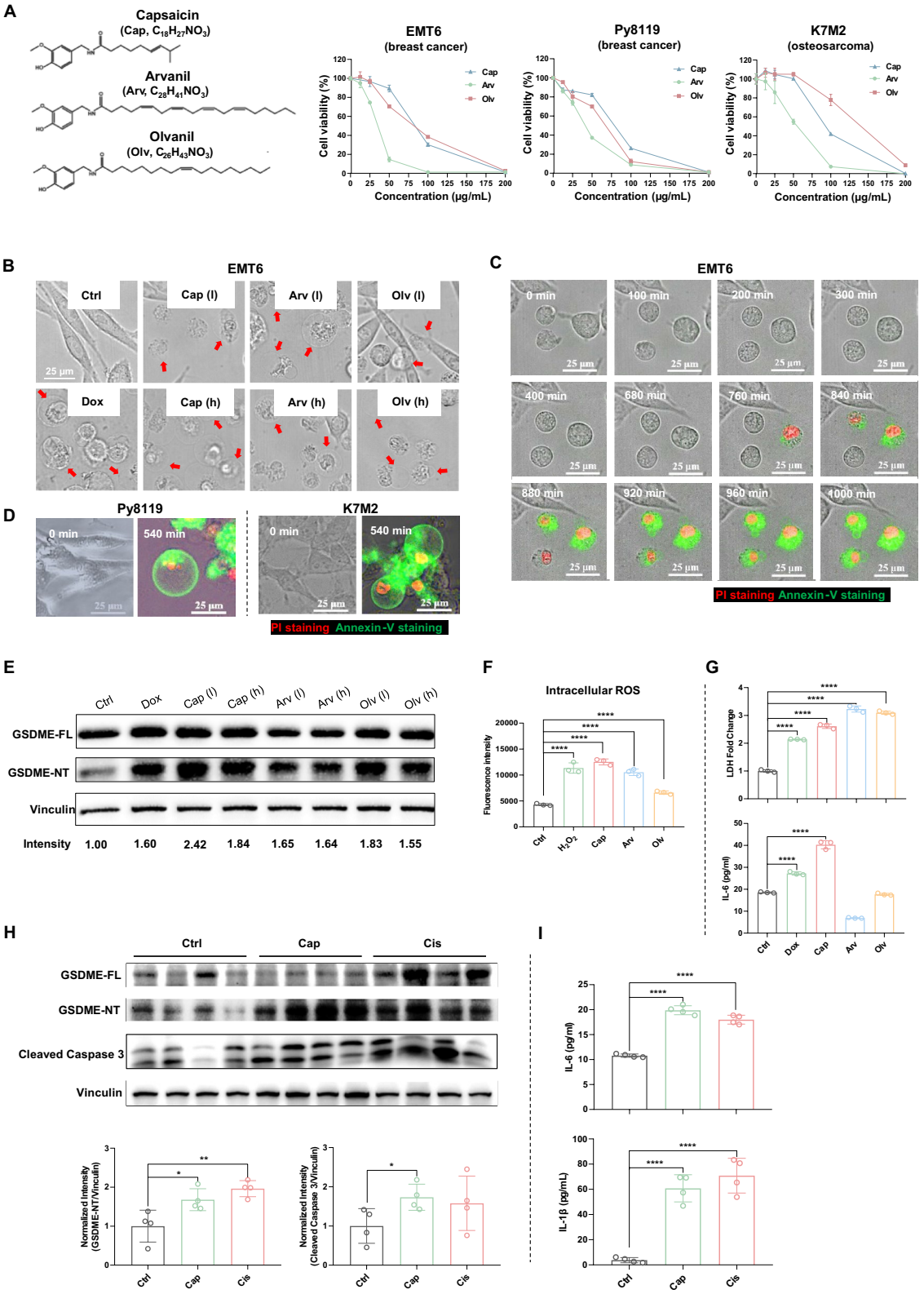

Fig. 1 (See legend on previous page.)

Results in Fig. 1F showed a significant increase in DCF fluorescence intensity following treatment with Cap and its analogs, particularly for Cap, indicating enhanced ROS production. This ROS elevation furtherly triggered caspase 3-mediated activation of GSDME (Figure S2), leading to membrane perforation and cell rupture, resulting in the release of lactate dehydrogenase (LDH) and interleukin-6 (IL-6), markers of membrane integrity loss and pro-inflammatory cytokine release [18, 20, 21]. Quantitative analysis in Fig. 1G revealed that Cap significantly increased LDH and IL-6 release compared to the control, underscoring its role in modulating immune response and inflammation. However, IL-6 induction by Arv and Olv was limited.

Considering the strong induction of pyroptosis by Cap in cancer cell lines, we further explored their capacity to induce pyroptosis in tumors within an intact animal model. EMT6 cell-bearing mice received intratumoral injections of 5 mg/kg Cap ($n = 4$). Cisplatin (Cis) served as a positive control for pyroptosis induction in vivo [22]. After 3 days, tumor tissues and mice serum were collected to assess pyroptotic markers. Proteins extracted from the tumor tissue were analyzed for GSDME-NT cleavage and cleaved caspase-3 expression levels. As shown in Fig. 1H, Cap treatment increased levels of GSDME-NT and cleaved caspase-3, confirming the activation of pyroptotic pathways at the tumor site. This activation was further supported by elevated levels of inflammatory factors IL-6 and IL-1β in mice serum, similar to the positive control of Cis (Fig. 1I).

Collectively, our findings demonstrate the potent pyroptotic activity of Cap both in vitro and in vivo in BC. We will investigate Cap's immunological therapeutic effects (Fig. 3) after confirming the GO-mediated ICD outcome in the same model (Fig. 2).

ICD effects of large-size, high C=O content GO in the EMT-6 breast cancer model

We aim to develop a nanocomplex that simultaneously induces pyroptosis and ICD. Given Cap's methoxybenzyl structure, we identified 2D nanomaterials, in this case, GO [23], as promising candidates. Our previous studies showed that the lateral size and carbonyl (C=O) content of GO significantly influenced its biological effects in macrophages [24]. Building on this, we evaluated GO's potential, as an ICD inducer, in cancer cells, assessing various GO samples (Fig. 2A) that differed in size (GO-1, GO-2, and GO-3) and C=O content (GO-3, GO-4, and GO-5) on EMT6 cells. Atomic force microscopy (AFM) and dynamic light scattering (DLS) data (Fig. 2B) confirmed the sheet-like structures of GO-1, GO-2, and GO-3, with average sizes of 459.36 ± 4.54 nm, 1105.6 ± 20.32 nm, and 1435.80 ± 80.78 nm, respectively, while their heights were similar at ~1 nm. The surface functional groups of GO-3, GO-4, and GO-5 were further characterized using X-ray photoelectron spectroscopy (XPS). As shown in Fig. 2C, the C1 s core-level spectra exhibited characteristic peaks at 284.6, 285.2, 286.8, 287.4, and 288.7 eV, corresponding to C–C/C=C, C–OH, C–O, C=O, and O=C–OH functional groups, respectively. XPS analysis also indicated varying C=O contents, approximately 15%, 10%, and 5% for GO-3, GO-4, and GO-5, respectively, while their sizes remained comparable (Figure S3). After a 24-h exposure to EMT6 cells, these GO samples induced significant cell killing. A significant correlation was observed between GO size (Fig. 2D, left panel) and C=O content (Fig. 2D, right panel) with cytotoxicity. GO with larger sizes or higher C=O content tended to be more cytotoxic to EMT-6 cancer cells. This finding was supported by the highest abiotic ROS generation by GO-3, which had the largest size and highest C=O content (Fig. 2E).

Considering the bigger lateral size that could also adsorb more Cap and the higher C=O content that could

(See figure on next page.)

Fig. 2 ICD effects induced by GO in vitro and in vivo. **A** Various GO samples from a range of sizes (GO-1, GO-2, and GO-3) and surface groups of C=O content (GO-3, GO-4, and GO-5) used in this study. **B** Representative AFM images (left panel) and DLS data (right panel) to demonstrate the sheet-like GO-1, GO-2, and GO-3 with an average size of ~500 nm, ~1000 nm, and ~1500 nm, respectively, with similar heights of 1 nm. **C** XPS data to show different surface groups and their content in GO-3, GO-4, and GO-5 samples, in terms of C=O contents with ~15%, ~10%, and ~5%, respectively. **D** Cell killing of GO samples and the correlation analysis between cytotoxicity and GO size (left panel) and C=O content (right panel). **E** H_2DCFDA assay to evaluate abiotic ROS generation of all GO samples. **F** Evaluation of the photothermal capacity of GO-3 to grow temperature (left panel) and kill EMT6 cells with NIR laser irradiation (808 nm, 1.7 w/cm^2, 5 min) (right panel). **G** Representative fluorescent images (left panel) and flow cytometry analysis (middle panel) showing CRT exposure, along with ELISA data (right panel) quantifying HSP70 levels in EMT6 cells treated with GO-3 and NIR light. Tunicamycin (Tun) was used as a positive control. The scale bar is 25 μm. **H** Quantification (left panel) and representative IHC staining images (right panel) for CRT as well as HMGB1 to confirm ICD induction in EMT6-bearing mice intratumorally injected 20 mg/kg GO under NIR irradiation 3 days late. The quantitative analysis was performed by calculating the percentage of integrated density across all areas in IHC images using ImageJ. Data represents mean ± SD, $n = 3$ for cell study and $n = 6$ for animal study. *** $p < 0.001$, **** $p < 0.0001$. The scale bar is 100 μm

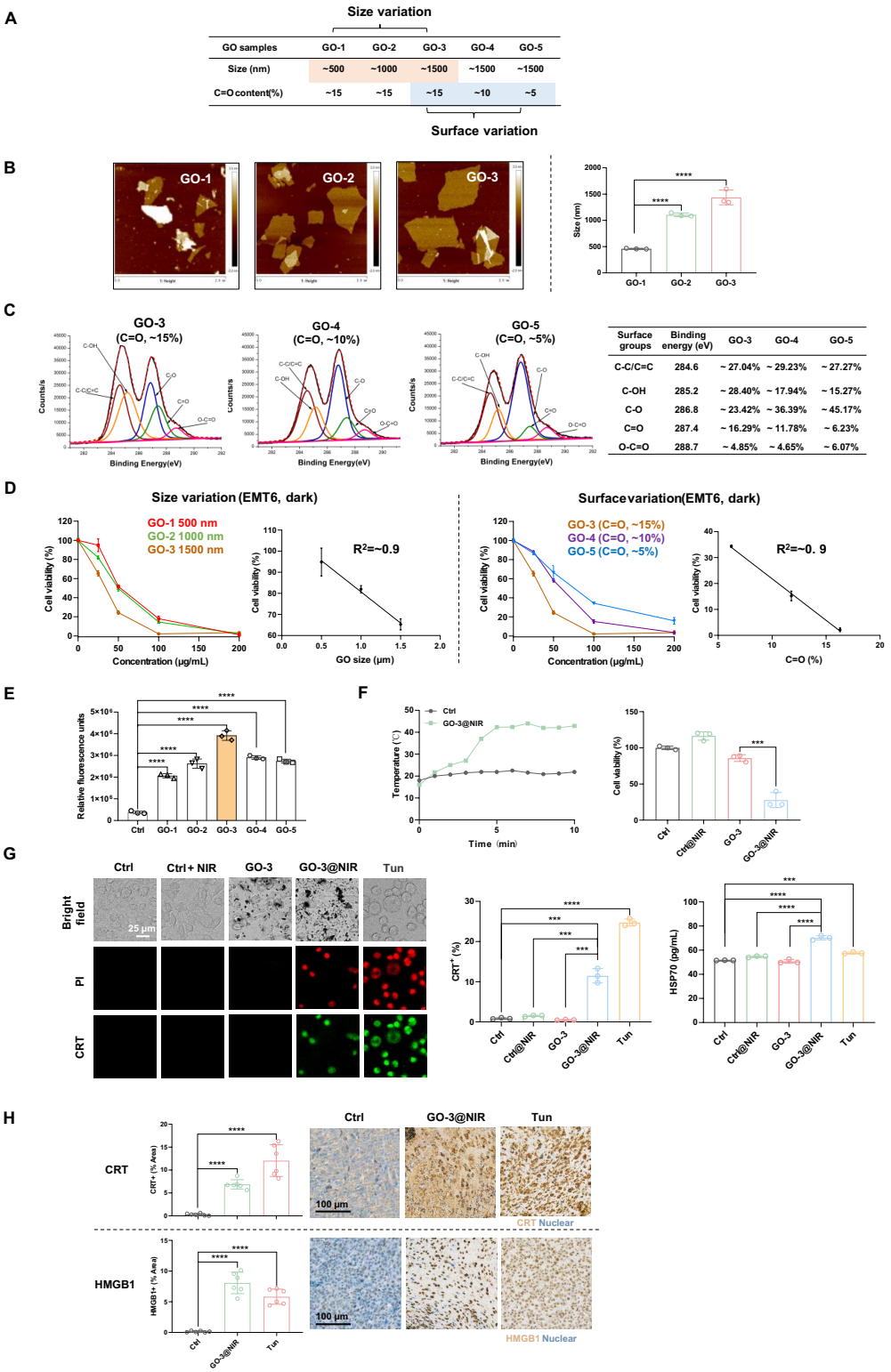

Fig. 2 (See legend on previous page.)

induce significant ROS generation to kill cancer cells, we, therefore, selected GO-3 to evaluate its ability to induce ICD effects. Under near-infrared (NIR) irradiation with 808 nm light for 5 min, GO-3 produced a substantial photothermal effect, raising the temperature to approximately 50 °C (Fig. 2F, left panel). This photothermal effect significantly enhanced GO-3-induced toxicity to cancer cells, increasing cell killing by ~60% compared to treatment without NIR light (Fig. 2F, right panel). To confirm that this enhanced cell killing was due to GO-3-mediated ICD, we assessed the key ICD marker CRT translocation to the cell membrane using immunofluorescent staining and flow cytometry in GO-treated EMT6 cells with/without NIR, respectively. As shown in Fig. 2G (left and middle panels), the combination of GO and NIR significantly induced CRT production, consistent with the positive control of ICD induction, tunicamycin (Tun). Additionally, other ICD markers, including HSP70 and HMGB1 release, were quantified using ELISA assays. As shown in Fig. 2G (right panel) and Figure S4, GO/NIR treatment significantly upregulated HSP70 and HMGB1 levels in EMT6 cells, further confirming its ICD-inducing effect.

Subsequently, we investigated the potential of GO-3 plus NIR to induce ICD effects in EMT6 tumor-bearing mice. The mice received intratumoral injections of 20 mg/kg GO-3 followed by 808 nm NIR radiation for 5 min. Tumor tissues were then collected and analyzed by immunohistochemical staining (IHC) to determine CRT and HMGB1, both markers of ICD. As demonstrated in our in vitro experiments, NIR alone lacks direct cytotoxicity and does not induce ICD unless combined with the photothermal agent GO (Fig. 2F, G). In line with the 3Rs principle of animal research (Replacement, Reduction, and Refinement), we did not include a NIR-only control in vivo. Further, the results in Fig. 2H showed that the GO-3 plus NIR treatment induced significant CRT translocation to the cell membrane and HMGB1 extracellular release in tumor areas. This pattern was similar to that observed with the positive control of ICD, Tun. Our findings collectively suggested that GO-3 could effectively induce ICD in vivo, promoting an enhanced immune response against the tumor.

Combining pyroptoic and ICD effects for synergistic antitumor effects

After establishing that Cap can trigger pyroptosis and that GO can induce ICD, we explored the synergistic potential of combining pyroptosis and ICD to achieve enhanced antitumor effects. The rationale behind this combination lies in the complementary mechanisms of action of Cap and GO [25–27]. Cap's aromatic rings interact with the π-electron system of GO via π–π stacking, while *Van der Waals* forces may also play a role in the adsorption process [25–27]. Additionally, GO's negative charge, due to its oxygenated groups, could electrostatically interact with positively charged or polar regions of Cap molecules (Fig. 3A). Using DLS and thin layer chromatography (TLC) [17], we first confirmed the presence of both Cap and GO in the physical Cap/GO complex, as evidenced by the decreased negative charge after GO incubation with Cap and the reduced Cap level in supernatant of nanocomplex during the adsorption process between 0 and 19 h (Fig. 3B). Further, the weight ratio of Cap to GO in the Cap/GO complex was determined to be approximately 1:2.

After synthesizing and characterizing the Cap/GO nanocomplex, we next evaluated its ability to simultaneously induce pyroptosis and ICD, two complementary and synergistic processes, using the aforementioned immunoblotting and IHC assays to detect corresponding markers. Although a definitive answer has not yet been determined, the co-induction of pyroptosis and ICD demonstrated a stronger response in vitro compared to using a single inducer alone. For example, the Cap/GO complex, designed to activate both pyroptosis and ICD, significantly upregulated GSDME-NT expression

(See figure on next page.)

Fig. 3 Characterization and assessment of the antitumor effect of the Cap/GO nanocomplex. **A** Scheme to demonstrate the synthesis of a Cap/GO nanocomplex due to the *π–π* stacking, electrostatic interaction, and *Van der Waals* forces between Cap and GO. **B** Characterization of the Cap/GO nanocomplex by DLS (left panel) and TLC (right panel). TLC was performed on supernatant samples utilizing a developing solvent system composed of ethyl acetate and hexane in a 2:1 ratio, with a sample volume of 2 µL applied to the plate. **C** Immunoblotting (left panel) and semi-quantitative results of IHC staining (middle and right panels) to demonstrate the simultaneous induction of pyroptosis and ICD by the Cap/GO nanocomplex, together with significantly elevated levels of GSDME-NT, CRT, and HMGB1 expression. **D** Cell viability study to demonstrate the Cap/GO nanocomplex-induced significant cancer cell killing than single Cap or GO treatment. **E** A treatment schedule in the antitumor vaccination experiment in mice. **F** Evaluation of tumor growth following EMT6 rechallenge on the contralateral side. Representative flow cytometry images (**G**) and corresponding quantification (**H**) showing the presence of mature dendritic cells (DCs), identified by CD11c, CD80, and CD86 positivity, in EMT6 tumor-bearing mice subjected to various treatments. **I** Schematic of timeline for the study in the efficacy experiment. EMT-6 tumor-bearing mice received indicated treatments. **J** Tumor volumes and weight recorded during the animal study. These data demonstrated the best-performing efficacy of the Cap/GO nanocomplex. **K** Body weight of mice during the animal study. **L** Quantification of the percentage (left panel) and IHC staining detail (right panel) of the $CD4^+$ T cells, $CD8^+$ T cells, and IFN-γ in EMT-6 tumor-bearing mice. * $p < 0.05$; ** $p < 0.01$; *** $p < 0.005$; **** $p < 0.001$. The scale bar is 100 µm

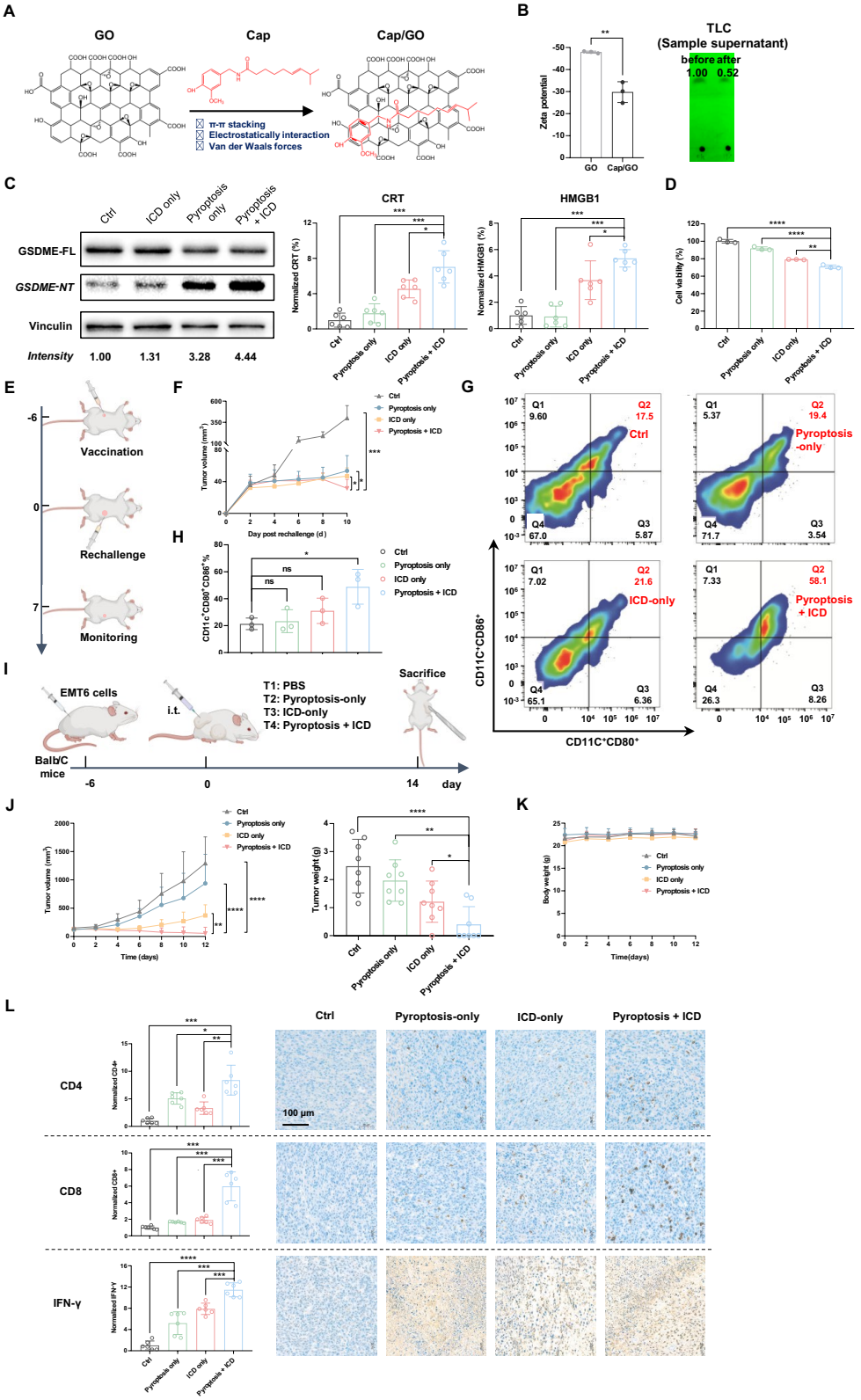

Fig. 3 (See legend on previous page.)

in EMT6 cells, an effect not observed with GO with NIR treatment (ICD-only) and notably stronger than that achieved with Cap alone (pyroptosis-only) treatment (Fig. 3C, left panel). Furthermore, the combined pyroptosis and ICD treatment markedly increased CRT and HMGB1 levels in EMT6-bearing mice, which were not elevated by pyroptosis-only treatment and showed a more potent effect than ICD-only treatment (Fig. 3C, middle and right panels; Figure S5). This simultaneous activation of pyroptosis and ICD by the 25 μg/mL Cap/GO complex also resulted in significantly higher cancer cell-killing effects than the same concentration of either pyroptosis-only or ICD-only treatment (Fig. 3D), highlighting the superior anticancer efficacy of combined pyroptosis and ICD induction over either treatment alone. These promising findings prompted us to further investigate the in vivo anti-tumor efficacy of the Cap/GO complex.

To demonstrate the therapeutic advantage of concurrently inducing pyroptosis and ICD, we first conducted a vaccination experiment using dying tumor cells treated with GO under NIR, Cap, or their combination [13, 28, 29]. EMT6 cells (1×10^6) were pretreated with 50 μg/mL of Cap for 24 h to induce pyroptosis, triggering a strong pro-inflammatory response that activates innate immunity. To generate ICD, an equal number of EMT6 cells were treated with 25 μg/mL of GO-3 nanoparticles and subjected to 5 min of NIR irradiation, enhancing antigen presentation and promoting adaptive immune activation. For the combined dying cell mixture, Cap-treated pyroptotic cells (5×10^5) were mixed with GO/NIR-treated ICD cells (5×10^5) to synergistically enhance both innate and adaptive immune responses, leading to a more robust and durable antitumor immunity compared to either treatment alone. These cell samples were then subcutaneously injected into the left flank of mice as a tumor vaccine, with PBS serving as the control group. Seven days later, untreated EMT6 tumor cells were introduced into the contralateral flank, as illustrated in Fig. 3E. Notably, vaccination with EMT6 cells preconditioned with either pyroptosis or ICD inducers alone was effective in providing tumor growth inhibition, demonstrating their individual functionality. However, mice vaccinated with EMT6 cells preconditioned with both inducers (pyroptosis + ICD) exhibited significantly enhanced tumor suppression, achieving more potent protection compared to single-inducer treatments ($p < 0.05$) (Fig. 3F). To investigate the underlying mechanism, these mice were sacrificed on day 11, and immune cells from tumor-draining lymph nodes (TDLNs) were isolated for immune analysis. Single-cell suspensions of the TDLNs were stained with fluorochrome-conjugated anti-mouse antibodies and analyzed by flow cytometry. The percentage of mature dendritic cells (DCs), characterized by CD11c, CD80, and CD86 positivity, was assessed. As shown in Fig. 3G, H and Figure S6, the percentage of mature DCs in the pyroptosis + ICD group (~48.8%) was significantly higher than in the control group (~21.3%), representing a 2.3-fold increase. This elevation in mature DCs suggests potential activation of T-cells, which could enhance the efficacy of cancer immunotherapy.

To further explore the synergistic therapeutic potential of the Cap/GO complex, we evaluated its anti-tumor effects in an EMT-6 tumor-bearing mouse model. The tumor-bearing mice received intratumoral injections of the Cap/GO complex, followed by 5 min of NIR radiation to raise the temperature to ~50 °C. For comparison, we included PBS, as well as single Cap and GO treatments as controls (Fig. 3I). As illustrated in Fig. 3J, significant differences were observed across the treatment groups. Notably, the combination therapy using pyroptosis and ICD inducers (Cap/GO complex) resulted in a pronounced reduction in both tumor volume (left panel) and tumor weight (right panel) compared to the single-inducer treatments, either pyroptosis-only (Cap) or ICD-only (GO-3 plus NIR). Additionally, tumor growth was markedly suppressed, with near-complete inhibition of progression. These results highlight the synergistic antitumor effect of the combination therapy, significantly enhancing overall treatment efficacy. Moreover, as shown in Fig. 3K, the body weights of mice remained stable across all treatment groups throughout the experimental period, with no significant weight loss detected.

To investigate the mechanisms underlying the observed anti-tumor effects, we analyzed the immune responses in the treated mice. As shown in Fig. 3L, immune marker expression varied significantly among the groups. Notably, the combination treatment group (pyroptosis plus ICD) exhibited significantly higher numbers of $CD4^+$ T cells and $CD8^+$ T cells compared to the control, pyroptosis-only, and ICD-only groups. Furthermore, the expression of IFN-γ, a critical cytokine in anti-tumor immunity, was markedly elevated in the combination treatment group. These findings collectively suggested that the concurrent induction of pyroptosis plus ICD robustly activated both innate and adaptive immune responses, contributing to its superb anti-tumor efficacy in the BC mouse model.

Biosafety assessment

Given the importance of nanosafety in potential clinical applications [30], we conducted a separate experiment to assess the biosafety of the Cap/GO complex. Healthy mice received various treatments through subcutaneous administration at equivalent cumulative doses, and blood biochemistry analyses were performed. As shown

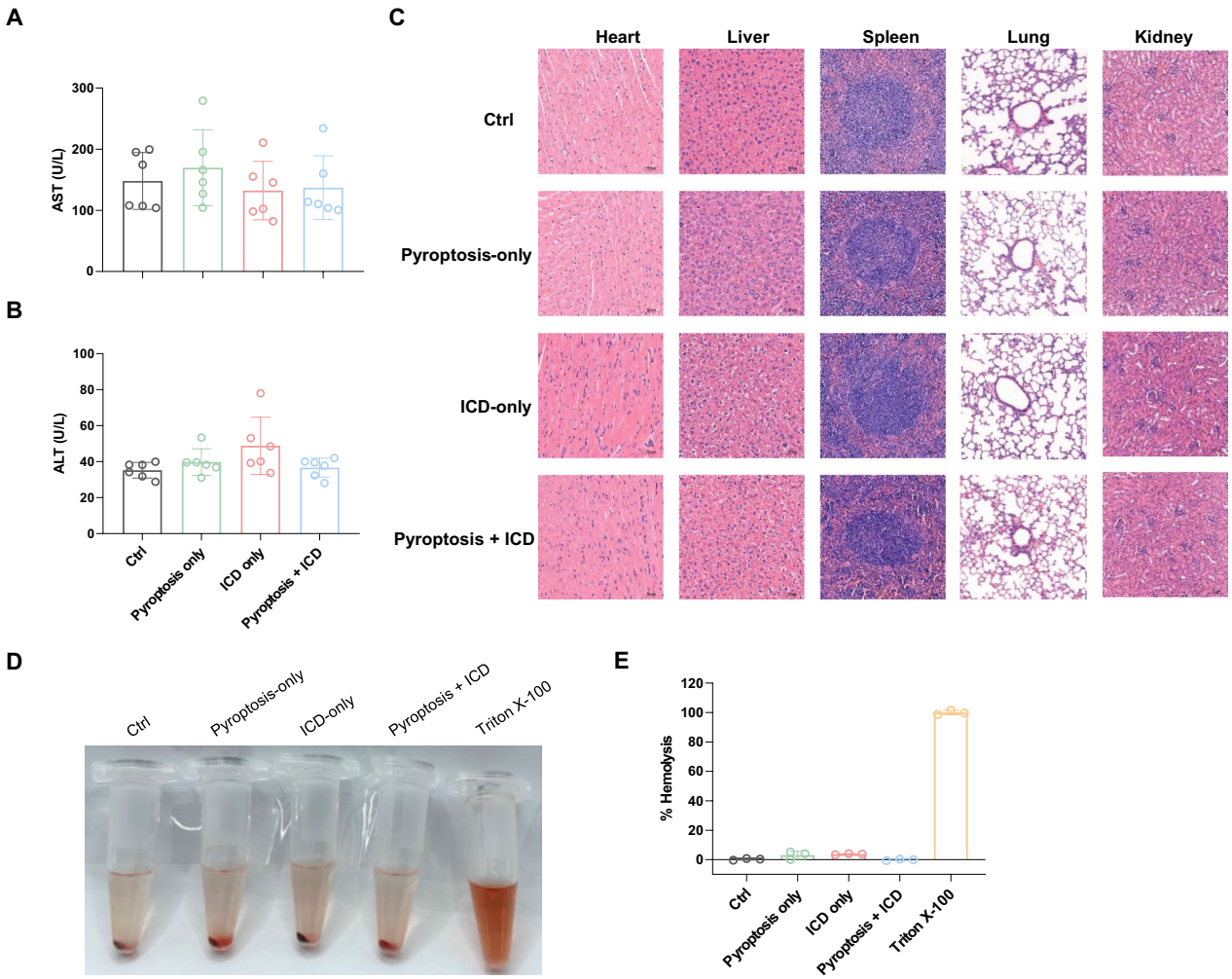

Fig. 4 Safety assessment of various treatments in healthy mice. **A - B** Plasma levels of AST (A) and ALT (B). **C** H&E staining of major organs after being injected with different indicated treatments. $n = 6$, Scale bars = 100 μm. **D** Representative images showing red blood cell (RBC) disruption, indicated by hemoglobin release in the supernatants of Eppendorf tubes. Triton was used as a positive control. **E** Quantification of hemolysis percentage for RBCs exposed to the tested materials

in Fig. 4A and B, key biochemical markers such as alanine aminotransferase (ALT) and aspartate aminotransferase (AST) exhibited no significant differences between the control and treatment groups ($p > 0.05$). This suggests that neither pyroptosis only, ICD only, nor their combination induced liver toxicity. Moreover, histological examination of major organs via H&E staining revealed no visible tissue damage in any of the experimental groups (Fig. 4C).

To evaluate the blood compatibility of the material, we conducted a hemolysis assay briefly, red blood cells (RBCs) were isolated from fresh mouse blood, incubated with the material, and hemolysis rates were quantified by measuring the absorbance of hemoglobin released into the supernatant at 540 nm. The results show that the hemolysis rate remains well below the 5% threshold recommended for biomaterial compatibility (Fig. 4D, E), confirming its excellent blood compatibility.

Together, these results demonstrate that the Cap/GO complex not only has potent anti-tumor effects but also maintains a favorable safety profile, underscoring its potential for further development as a therapeutic strategy.

Conclusion

This study demonstrates that the concurrent induction of ICD and pyroptosis by the Cap/GO nanocomplex significantly enhances breast cancer immunotherapy. This is achieved through the natural compound Cap, which induces pronounced cell membrane blebbing and

activates ROS-mediated cleavage of GSDME, ultimately triggering pyroptotic cell death. This process works synergistically with GO, which, when engineered with controlled physicochemical properties, effectively induces potent ICD under NIR irradiation. Importantly, the Cap/GO combination therapy demonstrated the best protection in a vaccination experiment, the strongest immunotherapeutic anticancer outcomes in the EMT6 mouse model, and a favorable biosafety profile. Our findings provide compelling experimental evidence supporting the simultaneous induction of pyroptosis and ICD as a novel and potent strategy for solid tumor treatment. This approach offers a promising alternative in the field of cancer immunotherapy, leveraging a synergistic mechanism to enhance anti-tumor efficacy and expand therapeutic options for breast cancer.

Experimental section

Materials

Capsaicin (PU0487-0025) was sourced from Chengdu Push Bio-technology Co., Ltd. Capsaicin analogs arvanil (Arv, GC10205) and olvanil (Olv, GC16467) were obtained from GlpBio Technology (Montclair, CA, USA). GO samples were purchased from Beijing Zhongkeleiming Daojin Technology Co., Ltd. The cell viability detection kit (CCK-8) was acquired from Mei Lun Biotechnology Co., Ltd, and H_2DCFDA (HY-D0940) was obtained from MedChemExpress. Antibodies for DFNA5/GSDME (ab215191), calreticulin (ab92516), and HMGB1 (ab79823) were obtained from Abcam. Additionally, the antibodies for CD4 [EPR19514] (ab183685), cleaved Caspase-3 (Asp175) (5 A1E, 9664), and calreticulin (D3E6 XP® Rabbit mAb, Alexa Fluor® 488 Conjugate, 62304 s) were purchased from Cell Signaling Technology. Antibodies for FITC anti-mouse CD11c (117306), PE/Cyanine7 anti-mouse CD80 (104734), and APC anti-mouse CD86 (105012) were purchased from BioLegend, Inc. CD8a Monoclonal Antibody (4SM15, 13–0808-82) and IFN gamma Monoclonal Antibody (XMG1.2, 14–7311-81) were sourced from Thermo Fisher Scientific Co., Ltd. Tunicamycin (T8480) was obtained from Solarbio Life Sciences Co., Ltd, and doxorubicin (S17092) was purchased from Shanghai Yuanye Bio-Technology Co., Ltd. Mouse ELISA kits for IL-6 (88–7064-88) and IL-1β (88–7013-22) were acquired from Thermo Fisher Scientific Co., Ltd.

Cell lines and animals

The EMT6 (mouse breast cancer) cell line was generously provided by Feng Shao from the National Institute of Biological Sciences, Beijing. The Py8119 (mouse breast cancer) cell line was a gift from Jie Yang and Junling Liu at Shanghai Jiao Tong University School of Medicine. The K7M2 (mouse osteosarcoma) cell line (1101MOU-PUMC000820) was purchased from the National Cell Line Resource in Beijing, China. These cell lines were maintained in DMEM supplemented with 10% FBS, 100 U/mL penicillin, and 100 μg/mL streptomycin at 37 °C in a humidified incubator with 5% CO_2. Female BALB/c mice, aged 6–8 weeks and weighing ~20 g, were procured from SPF Biotechnology Co., Ltd (Beijing, China) and were housed under a 12-h light–dark cycle at 22 °C, with food and water provided ad libitum.

Detection of Cap-mediated pyroptosis

Cells were treated with varying concentrations (0–200 μg/mL) of Cap, Arv, and Olv, and viability was measured 24 h post-treatment. Morphological changes in the cells were documented using a microscope. Pyroptotic cell death was characterized detailly through Annexin V/PI staining and analyzed using an Operetta High Content Screening System (Perkin Elmer) equipped with climate control (37 °C, 5% CO_2). The cleavage of GSDME to GSDME-NT was quantified by Western blotting, with vinculin serving as a loading control. Cytokine levels of IL-6 and IL-1β were determined using the commercial ELISA kits.

Characterization of GO-induced ICD effects

GO samples were characterized using AFM and DLS to assess their sizes, which were approximately 500, 1000, and 1500 nm for GO-1, GO-2, and GO-3. XPS was employed to analyze surface groups and to determine C=O content, which was found to be approximately 15%, 10%, and 5%, respectively, for GO-3, GO-4, and GO-5. The generation of ROS by GOs was evaluated using H_2DCFDA. The immunogenicity of GO under NIR irradiation (818 nm for 5 min) was assessed in EMT6 cells, with key ICD markers, such as CRT translocation and HMGB1 release, analyzed via immunofluorescent staining, flow cytometry, and immunohistochemistry (IHC) in both GO-treated EMT6 cells and mouse models.

Synthesis and characterization of the Cap/GO nanocomplex

The Cap/GO nanocomplex was synthesized by combining 2.5 mL of GO-3 at a concentration of 1 mg/mL with 2.5 mL of Cap, which was previously dissolved in DMSO to achieve the same concentration of 1 mg/mL. The mixture was stirred at room temperature for 19 h to promote physical adsorption between GO-3 and Cap. Following this, the solution was centrifuged at 15,000×*g* for 15 min to separate the Cap/GO nanocomplex from the supernatant.

The resulting precipitate was washed twice with deionized water to remove unbound capsaicin. DLS analysis

was then conducted to assess changes in the surface potential of both GO and the Cap/GO nanocomplex. Additionally, TLC was performed on supernatant samples collected at two time points: 0 h (before mixing) and 19 h (after mixing). The TLC analysis utilized a developing solvent system composed of ethyl acetate and hexane in a 2:1 ratio, with a sample volume of 2 μL applied to the plate. This analysis helped confirm the adsorption efficiency of capsaicin onto GO-3.

Assessment of the synergistic effects of the Cap/GO nanocomplex

EMT6 cells were treated with 25 μg/mL doses of Cap alone, GO alone, or the Cap/GO nanocomplex for a duration of 24 h. Following incubation, the GO-only and Cap/GO nanocomplex groups were subjected to 5 min of NIR radiation. Pyroptosis was then evaluated by analyzing GSDME-NT expression using WB assays, while CRT and HMGB1 levels, key ICD markers, in EMT6-bearing mice were assessed through immunohistochemistry (IHC). The cancer cell-killing efficacy of the treatments was further quantified using the CCK-8 assay.

A vaccination experiment was conducted using dying tumor cells treated with Cap, GO/NIR, or their combination. EMT6 cells (1.0×10^6) were pre-treated with 50 μg/mL of Cap for 24 h to generate pyroptosis-induced dying cells. ICD-induced dying cells were prepared using the same cell quantity, treated with GO/NIR at 25 μg/mL, followed by 5 min of NIR irradiation. A mixture of ICD- and pyroptosis-mediated dying cells was created by combining Cap-treated cells (5×10^5) with GO/NIR-treated cells (5×10^5). These cell samples were subcutaneously injected into the left flank of mice as a tumor vaccine, with PBS as the control group. Seven days later, untreated EMT6 tumor cells were introduced into the contralateral flank, and tumor sizes were monitored. To investigate the underlying mechanism, these mice were sacrificed on day 11, and immune cells from tumor-draining lymph nodes (TDLNs) were isolated for immune analysis. Single-cell suspensions of the TDLNs were stained with fluorochrome-conjugated anti-mouse antibodies (FITC anti-mouse CD11c, PE/Cyanine7 anti-mouse CD80, and APC anti-mouse CD86) and analyzed by flow cytometry. The percentage of mature dendritic cells (DCs), characterized by CD11c and CD86 positivity, was assessed.

The anti-tumor effects of the Cap/GO nanocomplex were evaluated in an EMT6 tumor-bearing mouse model. Tumor-bearing mice received intratumoral injections of the Cap/GO complex, followed by 5 min of NIR radiation to raise the temperature to approximately 50 °C. For comparison, PBS and individual treatments of Cap and GO were included as controls. Over approximately 14 days, tumor size, volume, and weight were monitored across treatment groups. Tumor tissues were analyzed for ICD markers (CRT, HMGB1), immune cell infiltration ($CD4^+$, $CD8^+$), and anti-tumor immunity (IFN-γ) through IHC staining. The semi-quantitative analysis of these markers was conducted by measuring the integrated optical density percentage across the entire area of IHC images using ImageJ.

Biosafety assessment

Healthy BALB/c mice (6 weeks old) were divided into four groups ($n = 6$). Each group received subcutaneous injections of saline, Cap, GO, or the Cap/GO complex at equivalent doses used in efficacy studies. All animals were euthanized 14 days post-treatment, and blood samples were collected for ALT and AST analyses. Major organs were fixed in 4% paraformaldehyde and subsequently embedded in paraffin for histological examination.

Statistical analysis

Statistical analyses were performed using GraphPad Prism 8.0 software. Data are expressed as mean and standard deviation (S.D.). One-way analysis of variance (ANOVA) and Student's *t* test were used to assess statistical significance. A p value of less than 0.05 was considered statistically significant (* $p < 0.05$, ** $p < 0.01$, *** $p < 0.005$, **** $p < 0.001$).

Supplementary Information

The online version contains supplementary material available at https://doi.org/10.1186/s12951-025-03439-2.

Additional file 1.

Additional file 2.

Author contributions

Silu Li (Data curation; Formal analysis; Investigation; Methodology; Validation; Writing—original draft) Jin Xin (Data curation; Formal analysis; Investigation; Methodology; Validation) Yumo Zhang (Data curation; Investigation; Methodology) Jidan Huang (Data curation; Investigation; Methodology) Haiqiang Wang (Data curation; Investigation; Methodology) Huan Meng (Conceptualization; Funding acquisition; Project administration; Resources; Supervision; Writing—review & editing) Jiulong Li (Conceptualization; Formal analysis; Funding acquisition; Project administration; Supervision; Writing—original draft; Writing—review & editing) Lin Zhu (Conceptualization; Funding acquisition; Project administration; Resources; Supervision; Writing—review & editing).

Funding

The authors acknowledge financial support from the National Key Research and Development Program of China (2022YFA1207300, 2021YFA1200902, and 2023YFC3403200). We want to thank the support from the National Natural Science Foundation of China (32201172 and 32271452), the Basic Science Center Project of the National Natural Science Foundation of China (22388101), the Strategic Priority Research Program of the Chinese Academy

of Sciences (XDB36000000), and the CAS Project for Young Scientists in Basic Research (YSBR-036).

Availability of data and materials
No datasets were generated or analysed during the current study.

Declarations

Ethics approval and consent to participate
All animal protocols were approved by the Institutional Animal Care and Use Committee of the National Center for Nanoscience and Technology (Approval No. NCNST21-2106-0608).

Competing interests
The authors declare no competing interests.

Author details
[1]Department of Pharmacy, The First Affiliated Hospital of Zhengzhou University, Zhengzhou 450052, Henan, People's Republic of China. [2]CAS Key Laboratory for Biomedical Effects of Nanomaterials and Nanosafety, CAS Center for Excellence in Nanoscience, National Center for Nanoscience and Technology (NCNST), Beijing 100190, People's Republic of China.

Received: 25 January 2025 Accepted: 4 May 2025
Published online: 27 May 2025

References

1. Guan P, Guo Z, Xu S, Lu H, Wang L, Gu Z, Liu Z. Molecularly imprinted nanobeacons redirect innate immune killing towards triple negative breast cancer. Angew Chem Int Ed. 2023;62: e202301202.
2. Bianchini G, De Angelis C, Licata L, Gianni L. Treatment landscape of triple-negative breast cancer—expanded options, evolving needs. Nat Rev Clin Oncol. 2022;19:91–113.
3. Debien V, De Caluwé A, Wang X, Piccart-Gebhart M, Tuohy VK, Romano E, Buisseret L. Immunotherapy in breast cancer: an overview of current strategies and perspectives. npj Breast Cancer. 2023;9:7.
4. Jin S, Muhammad N, Sun Y, Tan Y, Yuan H, Song D, Guo Z, Wang X. Multispecific platinum(IV) complex deters breast cancer via interposing inflammation and immunosuppression as an inhibitor of COX-2 and PD-L1. Angew Chem Int Ed. 2020;59:23313–21.
5. Nagata S, Tanaka M. Programmed cell death and the immune system. Nat Rev Immunol. 2017;17:333–40.
6. Yu P, Zhang X, Liu N, Tang L, Peng C, Chen X. Pyroptosis: mechanisms and diseases. Signal Transduct Target Ther. 2021;6:128.
7. Kroemer G, Galluzzi L, Kepp O, Zitvogel L. Immunogenic cell death in cancer therapy. Annu Rev Immunol. 2013;31:51–72.
8. Li J, Gao X, Wang Y, Xia T, Zhao Y, Meng H. Precision design of engineered nanomaterials to guide immune systems for disease treatment. Matter. 2022;5:1162–91.
9. Qiu X, Qu Y, Guo B, Zheng H, Meng F, Zhong Z. Micellar paclitaxel boosts ICD and chemo-immunotherapy of metastatic triple negative breast cancer. J Control Release. 2022;341:498–510.
10. Calvillo-Rodríguez KM, Mendoza-Reveles R, Gómez-Morales L, Uscanga-Palomeque AC, Karoyan P, Martínez-Torres AC, Rodríguez-Padilla C. PKHB1, a thrombospondin-1 peptide mimic, induces anti-tumor effect through immunogenic cell death induction in breast cancer cells. Oncoimmunology. 2022;11:2054305.
11. Bos PD, Plitas G, Rudra D, Lee SY, Rudensky AY. Transient regulatory T cell ablation deters oncogene-driven breast cancer and enhances radiotherapy. J Exp Med. 2013;210:2435–66.
12. Mei K, Liao Y, Jiang J, Chiang M, Khazaieli M, Liu X, Wang X, Liu Q, Chang CH, Zhang X, et al. Liposomal delivery of mitoxantrone and a cholesteryl indoximod prodrug provides effective chemo-immunotherapy in multiple solid tumors. ACS Nano. 2020;14:13343–66.
13. Galluzzi L, Vitale I, Warren S, Adjemian S, Agostinis P, Martinez AB, Chan TA, Coukos G, Demaria S, Deutsch E, et al. Consensus guidelines for the definition, detection and interpretation of immunogenic cell death. J Immunother Cancer. 2020;8: e337.
14. Bourne CM, Taabazuing CY. Harnessing pyroptosis for cancer immunotherapy. Cells. 2024;13:346.
15. Yang F, Xiao X, Cheng W, Yang W, Yu P, Song Z, Yarov-Yarovoy V, Zheng J. Structural mechanism underlying capsaicin binding and activation of the TRPV1 ion channel. Nat Chem Biol. 2015;11:518–24.
16. Basith S, Cui M, Hong S, Choi S. Harnessing the therapeutic potential of capsaicin and its analogues in pain and other diseases. Molecules. 2016;21:966.
17. Srinivasan K. Biological activities of red pepper (*Capsicum annuum*) and its pungent principle capsaicin: a review. Crit Rev Food Sci. 2016;56:1488–500.
18. Li F, Zhang X, Ho W, Tang M, Li Z, Bu L, Xu X. mRNA lipid nanoparticle-mediated pyroptosis sensitizes immunologically cold tumors to checkpoint immunotherapy. Nat Commun. 2023;14:4223.
19. Nel A, Xia T, Mädler L, Li N. Toxic potential of materials at the nanolevel. Science. 2006;311:622–7.
20. Mehrotra P, Maschalidi S, Boeckaerts L, Maueröder C, Tixeira R, Pinney J, Burgoa Cardás J, Sukhov V, Incik Y, Anderson CJ, et al. Oxylipins and metabolites from pyroptotic cells act as promoters of tissue repair. Nature. 2024;631:207–15.
21. Chen Z, Liu W, Yang Z, Luo Y, Qiao C, Xie A, Jia Q, Yang P, Wang Z, Zhang R. Sonodynamic-immunomodulatory nanostimulators activate pyroptosis and remodel tumor microenvironment for enhanced tumor immunotherapy. Theranostics. 2023;13:1571–83.
22. Wang Y, Gao W, Shi X, Ding J, Liu W, He H, Wang K, Shao F. Chemotherapy drugs induce pyroptosis through caspase-3 cleavage of a gasdermin. Nature. 2017;547:99–103.
23. Guo S, Garaj S, Bianco A, Ménard-Moyon C. Controlling covalent chemistry on graphene oxide. Nat Rev Phys. 2022;4:247–62.
24. Li J, Wang X, Mei K, Chang CH, Jiang J, Liu X, Liu Q, Guiney LM, Hersam MC, Liao Y, et al. Lateral size of graphene oxide determines differential cellular uptake and cell death pathways in Kupffer cells, LSECs, and hepatocytes. Nano Today. 2021;37: 101061.
25. Chao S, Zhao Y, Zhu Y, Zhou W, Zhu D, Liang Y, Li D, Wu Y, He Y, Xu J, Liu P. Intrinsically active capsaicin non-covalently modified nitrogen doped graphene for high-performance supercapacitors. J Electroanal Chem. 2023;929: 117131.
26. Zhai L, Li L, Zhang Q. Fabrication of capsaicin functionalized reduced graphene oxide and its effect on proliferation and differentiation of osteoblasts. Environ Toxicol Phar. 2018;57:41–5.
27. Veeman D, Shree MV, Sureshkumar P, Jagadeesha T, Natrayan L, Ravichandran M, Paramasivam P. Sustainable development of carbon nanocomposites: synthesis and classification for environmental remediation. J Nanomater. 2021;2021:5840645.
28. Wang H, Chen Y, Wei R, Zhang J, Zhu J, Wang W, Wang Z, Wupur Z, Li Y, Meng H. Synergistic chemoimmunotherapy augmentation via sequential nanocomposite hydrogel-mediated reprogramming of cancer-associated fibroblasts in osteosarcoma. Adv Mater. 2024;36:2309591.
29. Xiao W, Wang F, Gu Y,He X, Fan N, Zheng Q, Qin S, He Z, Wei Y, Song X. PEG400-mediated nanocarriers improve the delivery andtherapeutic efficiency of mRNA tumor vaccines. Chin Chem Lett. 2024;35:108755.
30. Li J, Chen C, Xia T. Understanding nanomaterial–liver interactions to facilitate the development of safer nanoapplications. Adv Mater. 2022;34:2106456.

Publisher's Note